Journal of Power Sources 220 (2012) 243–252

Contents lists available at SciVerse ScienceDirect

Journal of Power Sources

journal homepage: www.elsevier.com/locate/jpowsour

Active pore space utilization in nanoporous carbon-based supercapacitors: Effects of conductivity and pore accessibility

Mykola Seredych [a], Mikolaj Koscinski [a,b], Malgorzata Sliwinska-Bartkowiak [b], Teresa J. Bandosz [a,*]

[a] Department of Chemistry and CUNY Energy Institute, The City College of New York, 160 Convent Avenue, New York, NY 10031, USA
[b] The NanoBioMedical Centre, Faculty of Physics, Adam Mickiewicz University, Ulmotowskiego 85, Poznan 61-614, Poland

HIGHLIGHTS

- Pores smaller than 0.7 nm are the most active in charge storage in carbonaceous materials.
- Conductivity of carbon helps in efficient charge transfer to active pores.
- Polar groups help in charge transfer to the pores by increasing surface wettability.
- Active pore space utilization by DLC is affected by conductivity and wettability.

GRAPHICAL ABSTRACT

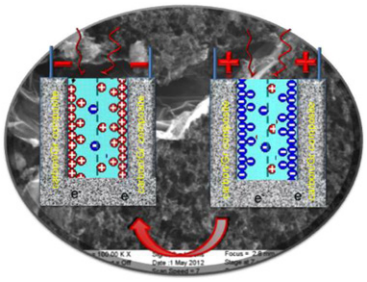

ARTICLE INFO

Article history:
Received 24 June 2012
Accepted 25 July 2012
Available online 8 August 2012

Keywords:
Capacitance
Nanoporous carbon
Graphene/carbon composite
Conductivity
Porosity

ABSTRACT

Composites of commercial graphene and nanoporous sodium-salt-polymer-derived carbons were prepared with 5 or 20 weight% graphene. The materials were characterized using the adsorption of nitrogen, SEM/EDX, thermal analysis, Raman spectroscopy and potentiometric titration. The samples' conductivity was also measured. The performance of the carbon composites in energy storage was linked to their porosity and electronic conductivity. The small pores (<0.7) were found as very active for double layer capacitance. It was demonstrated that when double layer capacitance is a predominant mechanism of charge storage, the degree of the pore space utilization for that storage can be increased by increasing the conductivity of the carbons. That active pore space utilization is defined as gravimetric capacitance per unit pore volume in pores smaller than 0.7 nm. Its magnitude is affected by conductivity of the carbon materials. The functional groups, besides pseudocapacitive contribution, increased the wettability and thus the degree of the pore space utilization. Graphene phase, owing to its conductivity, also took part in an *insitu* increase of the small pore accessibility and thus the capacitance of the composites via enhancing an electron transfer to small pores and thus imposing the reduction of groups blocking the pores for electrolyte ions.

1. Introduction

Porosity of activated carbons in combination with their surface chemistry is considered as main important factor governing their capacitive performance. This includes electrical double layer capacitance and pseudocapacitance, respectively [1–16]. While the former is based on the interactions of ions in the pores [1–7], the latter is strongly affected by functional groups on the carbon surface which impose Faradaic reactions and thus contribute to pseudocapacitance, especially in aqueous electrolyte [6,8–16]. Quinone/hydroquinone redox reactions and oxidation/reduction of negatively charged pyridinic and pyrrolic-like nitrogen were identified as the most important surface processes affecting

* Corresponding author. Tel.: +1 212 650 6017; fax: +1 212 650 6107.
E-mail address: tbandosz@ccny.cuny.edu (T.J. Bandosz).

0378-7753/$ – see front matter © 2012 Elsevier B.V. All rights reserved.
http://dx.doi.org/10.1016/j.jpowsour.2012.07.074

pseudocapacitance of carbons [8–10,13,15,16]. While the typical capacitance of activated carbons is about 100 F g^{-1} via various surface modification methods and improved activations the capacitance values over 300 F g^{-1} in aqueous electrolytes has been reported [6–14].

Other factors besides porosity and surface chemistry, which strongly affect the capacitive behavior are wettability and conductive properties [17–20]. To enhance the electrical conductivity of electrodes conductive graphite or carbon black are added to the carbon electrodes. The conductive properties can be also enhanced by addition of carbon nanofibers [21,22] carbon nanotubes [23,24] and graphene [25,26]. The latter has been recently extensively explored and contradictory results have been reported. While Totir and coworkers clearly indicated the negative effects of its addition to activated carbons [27], Buglione and Pumera showed that the composites of graphene and carbon nanotubes exhibit merely arithmetic average of the capacitance of the individual components [28]. In another study of the latter authors the dramatic influence of the graphene preparation on the capacitive performance was analyzed [29,30]. Recently, we have shown that the addition of graphite oxide (GO) to the nanoporous carbon precursor and its reduction during carbonization, followed by further reduction of the resulting composite did not increase the performance noticeably [31]. Only the volume of small pores similar in sizes to the solvated ions was found as the most important for the overall performance.

To further investigate the influence of porosity and conductivity on the capacitive performance the detailed study of the electrochemical behavior of nanoporous carbon composites obtained by *insitu* carbonization of organic polymer (specific sodium salt) in the presence of the commercial graphene phase was performed. To clarify our objective we would like to point out that we do not intend to present the best performing materials. We attempt to find the clearer indication of the specific effects of the porosity, surface chemistry and conductivity on the capacitive behavior of such complex systems as nanoporous carbon composites.

2. Experimental details

2.1. Materials

Poly(4-styrenesulfonic acid-co-maleic acid) sodium salt (PS) was used as a nanoporous carbon precursor. The powdered polymer was carbonized at 800 °C for 40 min under nitrogen, in a horizontal furnace. The details on the initial sample preparation are described in Ref. [32]. This sample is referred to as C-I. The composites, which are addressed here for the first time, were synthesized by mixing the amount of polymer corresponding to 95 or 80% of resulting nanoporous carbons (calculated taking into account the yield of C-I carbon) with 5 or 20% of graphene (Gr) (METSS corporation), respectively. The resulting composites were washed in water in a Soxhlet apparatus to remove an excess of water-soluble inorganic salts. They are referred to as CGr5-I and CGr20-I where 5 and 20 corresponds to the percentage of Gr in the composite.

The subsamples of nanoporous carbon and composites obtained at 800 °C were heated at 950 °C for 1 h in nitrogen. The heating rate was 10 °C min^{-1}. The materials obtained are referred to as C-II, CGr5-II, and CGr20-II.

2.2. Methods

2.2.1. Electrochemical measurements

The capacitive performance of all carbon samples was investigated in 1 M H_2SO_4 and 0.5 M Na_2SO_4 using two- and three-electrode cells. The working electrode was prepared by mixing the active material with polyvinylidene fluoride (PVDF) and commercial carbon black (carbon black, acetylene, 50% compressed, Alfa Aesar) (8:1:1) in N-methyl-2-pyrrolidone (NMP) until homogeneous slurry. The slurry was coated on a Ti foil (current collector) with the total surface area of 1 cm^2 of an active material. The electrodes were dried at 120 °C for 24 h and then weighted. The total mass was between 6 and 9 mg and two electrodes with identical weight were selected for the measurements.

Cyclic voltammetry and galvanostatic charge–discharge were used in evaluation of the capacitive performance. The measurements were carried out using VersaSTAT MC (AMETEK, Princeton Applied Research) within the potential window of 0 V–1 V for 1 M H_2SO_4 and −1 V to 1 V for 0.5 M Na_2SO_4 with the scanning rate of 5 and 100 mV s^{-1} (cyclic voltammetry) and the current loads of 50, 100 mA g^{-1} and 1 A g^{-1} (galvanostatic charge/discharge).

Cyclic voltammetry at the scan rate of 5 mV s^{-1} was also recorded in a three-electrode cell using the Ag/AgCl reference electrode and active material as a working electrode and platinum rod as a counter electrode, respectively.

The gravimetric capacitances (C_g) were calculated from the discharge curves according to the Equation:

$$C_g = \frac{I^*\Delta t}{\Delta E^* m} \quad (1)$$

where I (A g^{-1}) is the current load; Δt (s) is the discharge time and ΔE (V) is the potential window. The gravimetric capacitances of materials studied are reported here as the specific gravimetric capacitance per one electrode.

The values of the specific capacitance (F g^{-1}) were also estimated by cyclic voltammetry (scan rate of potential 5 mV s^{-1}). The specific capacitance was calculated according to the Equation:

$$C = Q/(\Delta E^* m) \quad (2)$$

where Q is the charge obtained after integrating the voltammogram, m is the total mass of electrode, and ΔE is the potential window.

2.2.2. Potentiometric titration

Potentiometric titration measurements were performed with a DMS Titrino 716 automatic titrator (Metrohm). The details on the experiments are included in Supplementary Information. The experimental data was transformed into a proton binding curves, Q, representing the total amount of protonated sites. From them the pK_a distributions were calculated [33,34].

2.2.3. Evaluation of porosity

Sorption of nitrogen at its boiling point was carried out using ASAP 2020 (Micromeritics, Surface area and porosity analyzer). Before the experiments, samples were out-gassed at 120 °C to constant vacuum (10^{-4} Torr) which took between 12 and 24 h. The surface areas (BET method), total pore volumes, V_t, (from the last point of isotherm at relative pressure equal to 0.99), volumes of micropores, V_{mic}, volume in pores less than 0.7 nm and less than 1 nm, $V_{<0.7nm}$ and $V_{<1nm}$, mesopore volumes, V_{mes}, along with pore size distributions (PSDs) were calculated from the isotherms. The last five quantities were calculated using density functional theory, DFT [35].

2.2.4. SEM/EDX

Scanning electron microscopy (SEM) images were performed at Zeiss Supra 55 VP. The accelerating voltage was 5.00 kV. Scanning was performed insitu on a sample powder without coating.

Electron-dispersive X-ray spectroscopy (EDX) analysis was done at magnification 10 KX and the content of elements on the surface was calculated.

2.2.5. DC conductivity measurements

The DC conductivity was measured on the polymer-based carbon and composites graphene/carbon pellets with the same composition as that used to make the electrodes (see description in Electrochemical Measurements). The prepared powder was pressed by a Carver Press machine applying 2 tons pressure and disk-shaped well-packed pellets with diameter 8 mm were formed. The pellets were dried in oven for 12 h. The pellets' thickness was measured by a spring micrometer. The measurement of conductivity was carried out by the Keithley 2400 multimeter. The experimental details are included in Fig. S1 of Supplementary Information.

3. Results and discussion

The measured CV curves for the composites in a two electrode cell in H_2SO_4 and Na_2SO_4 as electrolytes are collected in Figs. 1 and 2, respectively. The shapes, especially at low scan rate are rectangular indicating an ideal capacitor behavior. With an increase in the scan rate the deviation from the rectangular shapes are noticed and they are the most pronounced for the CGr20 samples. These deviations increase with an increase in scan rate and are caused by the kinetic limitations in charge transfer. They are expected to be more pronounced for the materials with small pores. When the performance at 5 mV s^{-1} is analyzed the composites obtained at 950 °C show the most deviations from the capacitive behavior. Even though the scan rate is rather small, the treatment in 950 °C could open the very small pores difficult to access by electrolyte ions and thus improves the capacitance [20]. The improvement after charge/discharge can be the result of carbon surface "activation" during this process.

The charge/discharge profiles (Fig. 3) were used to calculate the gravimetric capacitance. They are triangular in shape and exhibit only small Ohmic drops at high currents related to the resistivity of the cells. The values and the capacitance retention ratios are collected in Table 1. As expected, the capacitance in H_2SO_4 is almost twice of that in Na_2SO_4. In the former electrolyte the pseudocapacitance is expected when functional groups are present on the surface of our materials [20]. Moreover, if small pores are present, the minute differences in the sizes of ions can play a critical role and smaller ions should lead to a larger capacitance. Interestingly, the capacitance values measured for all materials obtained at 800 °C are similar regardless the amount of Gr added. No significant differences are observed for the samples heated at 950 °C, however the performance for the composites decreased about 10%. Similar behavior is found in Na_2SO_4. In this electrolyte an addition of

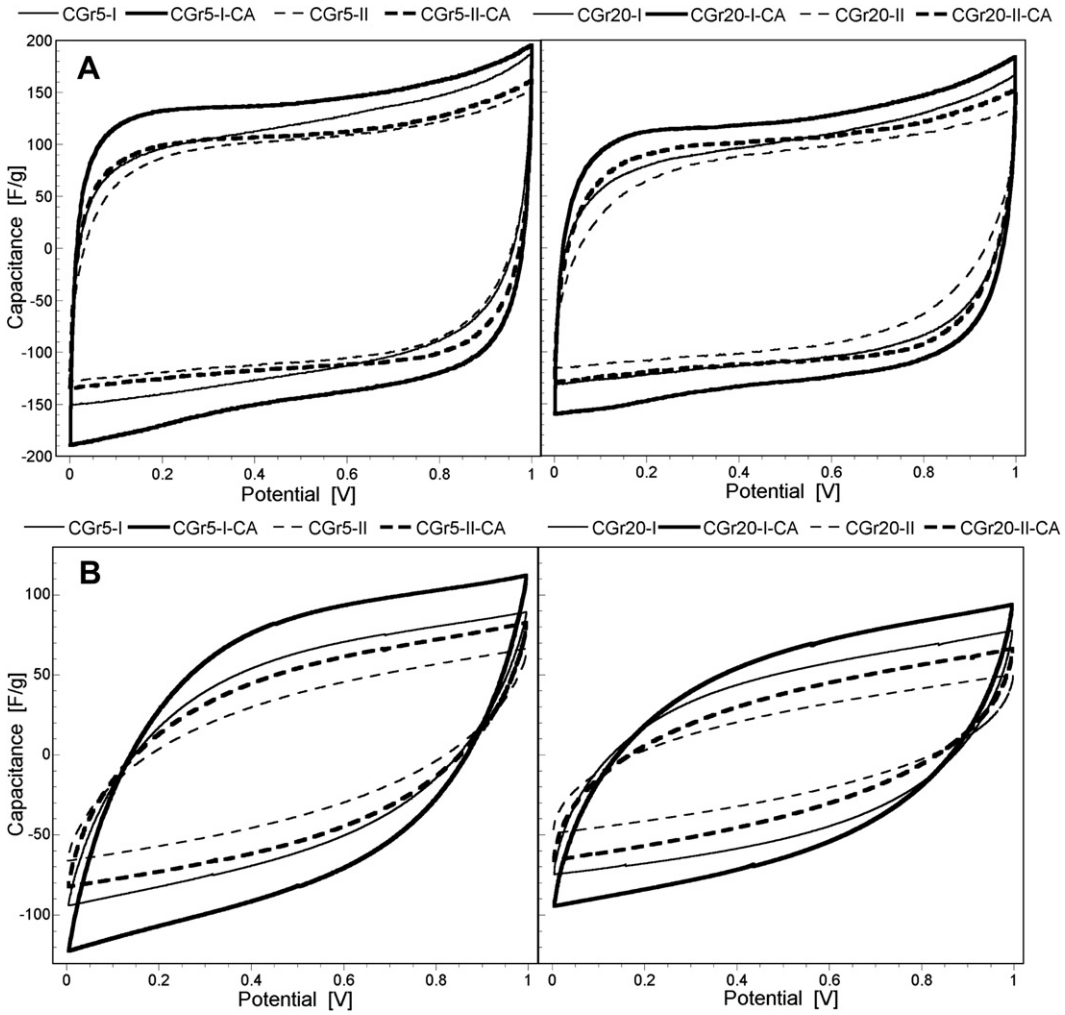

Fig. 1. CV curves in two electrode cell at different scan rates in 1 M H_2SO_4 as the electrolyte: 5 mV s^{-1} (A) and 100 mV s^{-1} (B).

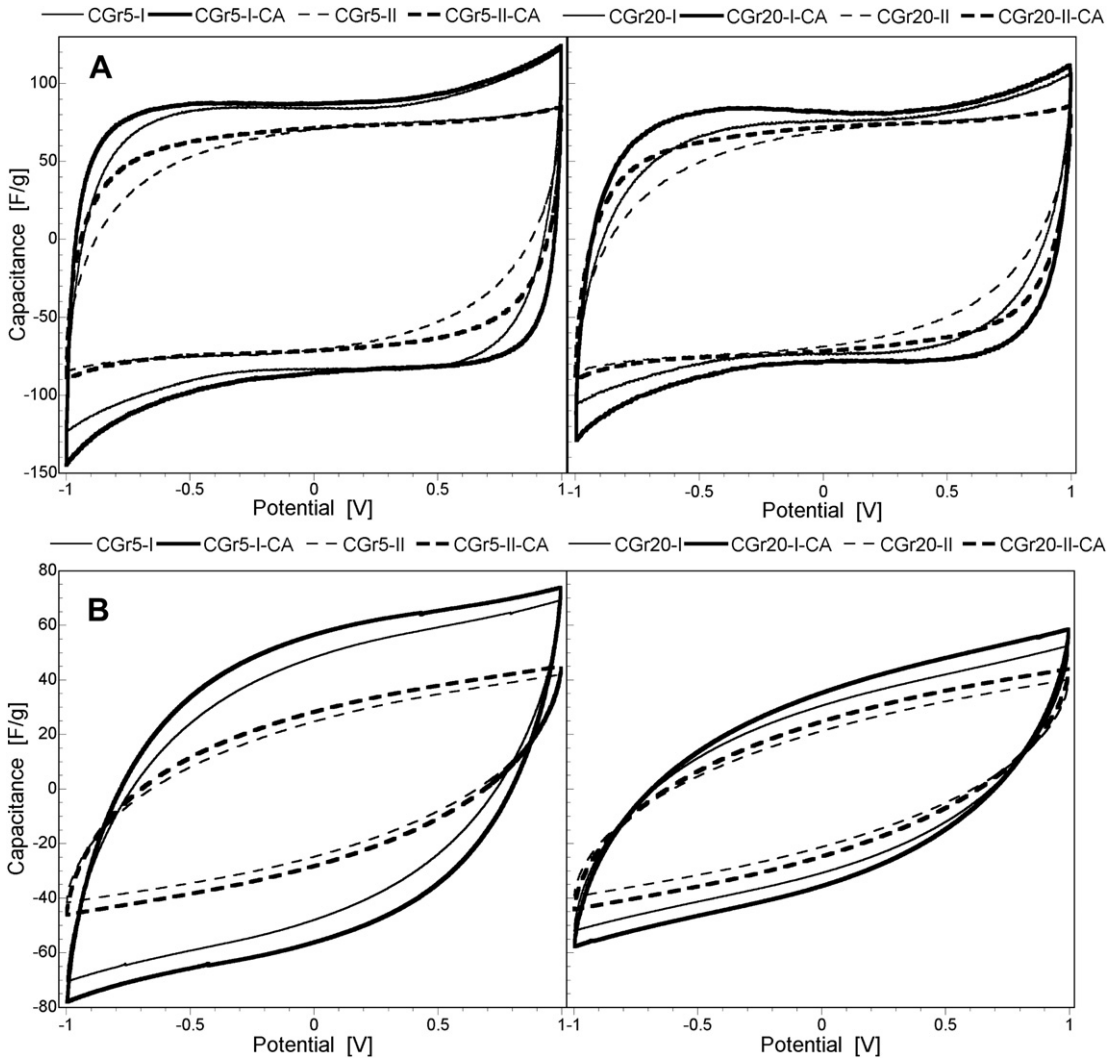

Fig. 2. CV curves in two electrode cell at different scan rates in 0.5 M Na_2SO_4 as the electrolyte: 5 mV s^{-1} (A) and 100 mV s^{-1} (B).

graphene for the composite heated at 950 °C, regardless its amount, decreased the capacitance about 20% compared to the parent carbon. On the other hand, the effect of graphene addition is seen on the capacitance retention ratio. It decreases with an increase in the graphene content and an increase in the treatment temperature. This might be related to the increase in surface hydrophobicity to which graphene phase is expected to contribute.

This peculiar behavior of the composites can be explained by analyzing the surface properties of the composites and variation in these properties are imposed by addition of the graphene phase. The comparison of the pore size distribution for all materials is presented in Fig. 4. They were calculated from nitrogen adsorption isotherms, whose shapes indicate the micro–mesoporous nature of our materials. Apparently an addition of the graphene phase significantly affects the volume of pores between 1 and 3 nm. Their volume visible decreased, regardless of the graphene content. On the other hand, the addition of 5% Gr significantly increases the volume of very small pores, of about 0.5 nm in diameter, and decreases the volume of pores with sizes of about 1 nm. The volume of the latter pores, even though it decreases for CGr20-I compared to C-I, is higher for the composite with the higher content of graphene. Heat treatment at 950 °C generally decreases the volume of pores smaller than 1 nm, which must be related to an increase in the carbon aromatization degree. The increase in aromatization degree is also expected to result in a decrease in pore sizes. That decrease is reflected on the deviation from the rectangular shape observed for CV curves of these composites discussed above. One has to remember that the porosity is determined by the nitrogen molecule so all pores which are smaller than nitrogen (0.36 nm) or similar to its size are not visible owing either to sieving effects or kinetic limitation for nitrogen to enter them.

The parameters of the porous structure are collected in Table 2. The surface areas for the initial composites are half of those obtained for the C-I carbon and no trend with the variation in the amount of graphene added is found. While the heat treatment does not affect the initial carbon, a significant decrease in the surface of the composites is found, especially for CGr20-II (over 20%). About 20% decrease in the volume of pores is also detected. Those changes must be related to the mechanism of carbonization and the thermal stability of the graphene phase. As opposite to the graphite oxide, whose layered structure has been already altered by oxidation, graphene is expected to be unaffected by the pore formers (gases and sodium released during carbonization [31,32]). Therefore, its layers should introduce strong constrains for development of porosity in the carbon phase and the pores formed are expected to be small in size and of lower volume. It is interesting that no

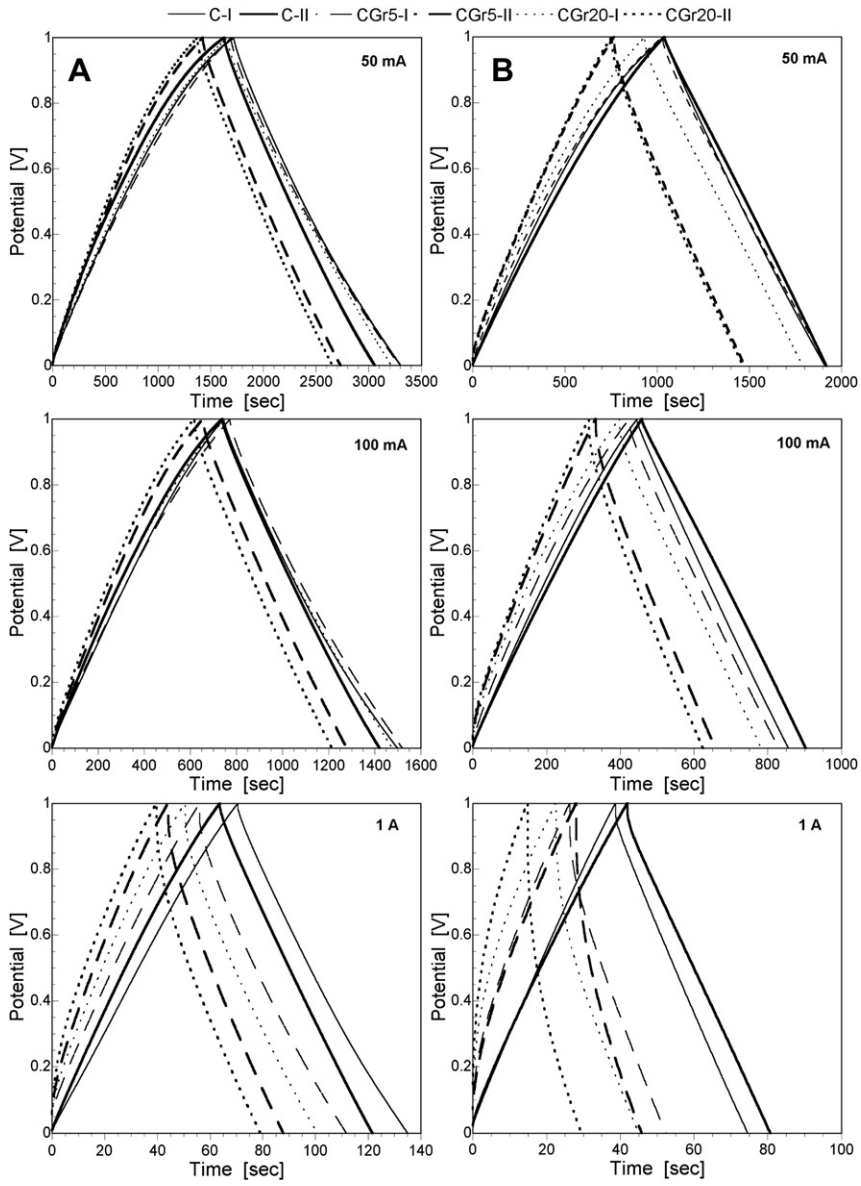

Fig. 3. Charge–discharge curves at different current loads in H_2SO_4 (A) and Na_2SO_4 (B).

Table 1
Gravimetric capacitance values, C_g, at different current loads, capacitance retention ratio, C_g retention, the specific capacitance calculated from the CV curves in two electrode cell before, Cg2C-a, and after the charge/discharge measurements, Cg2C-b.

Sample	C_g (F g^{-1})			C_g retention (%)	Specific capacitance (F g^{-1})	
	50 mA g^{-1}	100 mA g^{-1}	1 A g^{-1}		Cg2CV-a	Cg2CV-b
H_2SO_4						
C-I	158	150	130	82	139	141
C-II	143	137	118	82	125	124
CGr5-I	160	151	119	74	116	141
CGr5-II	131	126	93	71	101	110
CGr20-I	155	147	107	69	102	124
CGr20-II	129	121	84	65	87	102
Na_2SO_4						
C-I	87	82	75	86	89	90
C-II	90	89	80	89	90	90
CGr5-I	89	82	57	64	83	89
CGr5-II	71	67	44	62	63	66
CGr20-I	85	78	52	61	72	81
CGr20-II	72	64	34	47	62	67

decrease in the porosity is found when more graphene is added. The only plausible explanation at this stage of our study is the lower dispersion of graphene phase in terms of the number of graphene flakes than in the case of 5% addition. Owing to the high viscosity of the polymeric precursor, 20% graphene may form aggregates built of the large number of stacked layers. A decrease in the porosity caused by heating at 950 °C can be the result of an increase in the aromatization level of the amorphous carbonaceous materials.

The texture of the composites is presented on SEM images in Fig. 5. As seen they represent a type physical mixture of graphene flakes and amorphous porous carbon phase. Some graphene layers are covered by porous carbon. Overall CGr5 seems to be more porous with larger domains of the carbon phased than CGr20.

The mentioned above differences between the nanoporous carbons and the composites are seen on DTG curves (Fig. S2 of Supplementary Information). The chemistry of the composites obtained at 800 °C is similar to that of carbon and the decomposition of sulfonic and carboxylic groups is seen as a well-defined peak at temperatures less than 500 °C [36,37]. Carboxylic groups

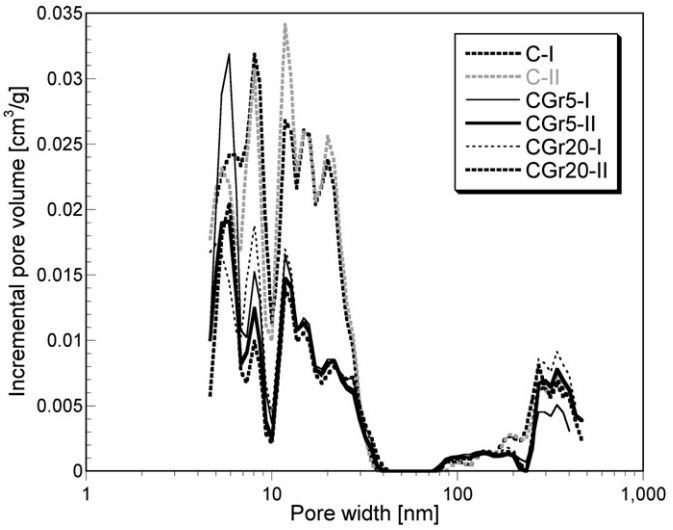

Fig. 4. Pore size distributions for the materials studied.

can be also transformed during heat treatment into form of quinone or pyrone type oxygen [37]. The basic groups decompose as a broad peak between 500 and 900 °C. Treatment at 950 °C results in almost "clean" C-II carbon but the composite still show the well-defined low and high temperature peaks related to the lower degree of aromatization. The latter, at about 650 and 850 °C represent decomposition of basic groups, which in the form of quinone/hydroquinone may increase the capacitive performance by the contribution to Faradaic reactions [38]. The broadness of the peaks suggests high chemical heterogeneity related to the oxygen species. Their redox reactions in sulfuric acid can contribute to pseudocapacitance [20] and thus to the larger capacitance measured in this electrolyte.

Even though the aromatization level of the amorphous composite component can be lower in the composites than that in the nanoporous carbon, on the average, the structure of the composites can exhibit less defects than the C-I carbons. The comparison of the Raman spectra is presented in Fig. S3 of Supplementary Information. As expected for this kind of materials two bands, G and D, are found at 1600 cm^{-1} and 1360 cm^{-1}. While the former is the only line observed for pristine graphite-type structure, the latter is induced by disorders in the graphene/carbon structure. The ratio of the intensity of the I_D to I_G bands for the initial samples is listed in Table 3. This ratio, when higher, indicates the higher degree of defects in the carbonaceous materials [39]. Addition of graphene visibly decreases the ratio for the composites and for CGr20 it is close to that found for the commercial graphene.

The results of chemical analysis show the difference in the surface content of elements (Table 3). Heating the C-I carbon at 950 °C decreases the content of oxygen and sulfur. Nevertheless, these species are still deposited on the surface. Supporting for the hypothesized above differences in the mechanism of carbonization caused by the presence of graphene layers is the very high content of oxygen in the composites, especially with 20% graphene. Some of these oxygen groups likely contribute to the pseudocapacitance [20]. The composites also contain much more sulfur on the surface than the parent nanoporous carbon and in CGr5-I some residual sodium is present. It is removed when the sample is heated at 950 °C [40]. Owing to the temperature of heat treatment, the majority of sulfur should be in thiophenic compounds [36,41], although some sulfone or sulfoxide can be also present [36].

Table 3 also contains the amounts of acidic groups detected by potentiometric titration. Although the pK_a distributions were obtained with the detailed numbers of groups represented by each pK_a (Fig. S4 and Table S1 of Supplementary Information) here we report only the number of strongly acidic ($pK_a < 7$), weakly acidic ($pK_a > 7$) and the total number of groups. Medium acidic surface groups at pK_a between 4.8 and 6.3 are assigned to second and higher dissociation constants of multibasic carboxylic acids, and carbonyl, lactone-type structure. Carbonyl groups can be transformed into keto–enol structure. Weak acidic surface groups with pK_a between 8.0 and 10.2 are assigned to differently substituted phenol (hydroquinone) and keto (quinone) structure [42,43]. The results are in agreement with those discussed above based on the thermal analysis. Thus C-I is the most acidic with the almost even number of strongly acidic and weakly acidic species. Its heating at 950 °C significantly decreases the amounts of strong acids on the surface. The composite with 5% graphene has much more of the weakly acidic groups than the parent carbon and heat treatment does not affect their number. Similar pattern is found for the CGr20 samples although they have much less acidic groups on the surface. These results in conjunction with EDX surface analysis suggest that the significant amount of oxygen groups are located on the external surface of the composites and a marked amount of that oxygen does not exhibit the pK_a in our experimental window. Therefore combining the elemental analysis, thermal analysis, and potentiometric titration results it can be deducted that ketone, ether, quinone configuration or sulfoxide/sulfone are present on the surface. Their redox reactions in acidic electrolyte contribute to the pseudocapacitance.

To see the effect of Faradaic reactions, the CV curves were measured in three electrode cell. The examples of CV at scan rate 5 mV s^{-1} are presented in Fig. 6. The trend in the general shape and areas of the curves is similar to that observed in two electrode cell. Besides, in three electrode cells Faradaic reactions can be visible. For the experiments run in H_2SO_4 humps from reversible redox reactions are seen at the potential of 0.58 V *vs* Ag/AgCl. Then the irreversible hump is seen at about 0.2 V *vs* Ag/AgCl. That irreversible process decreases with an addition of Gr and can be related to the reduction of strongly acidic carboxylic groups, sulfonic and sulfone present on our materials. Owing to the developed surface chemical heterogeneity of these samples, the overlap of the redox humps cannot be crossed out and many subsequent Faradaic

Table 2
The parameters of porous structure calculated from nitrogen adsorption measurements and pellets' conductivity, σ.

Sample	S_{BET} (m^2 g^{-1})	V_t (cm^3 g^{-1})	V_{mes} (cm^3 g^{-1})	$V_{<0.7nm}$ (cm^3 g^{-1})	$V_{<1nm}$ (cm^3 g^{-1})	V_{mic} (DFT) (cm^3 g^{-1})	σ [S m^{-1}]
Gr	56	0.151	0.149	0.000	0.000	0.002	826
C-I	1386	0.904	0.463	0.140	0.232	0.441	14.4
C-II	1347	0.958	0.510	0.143	0.218	0.448	16.9
CGr5-I	775	0.540	0.269	0.134	0.172	0.271	123.1
CGr5-II	643	0.496	0.280	0.094	0.123	0.216	102.3
CGr20-I	783	0.608	0.364	0.101	0.145	0.244	209.2
CGr20-II	594	0.493	0.298	0.085	0.108	0.195	211.9

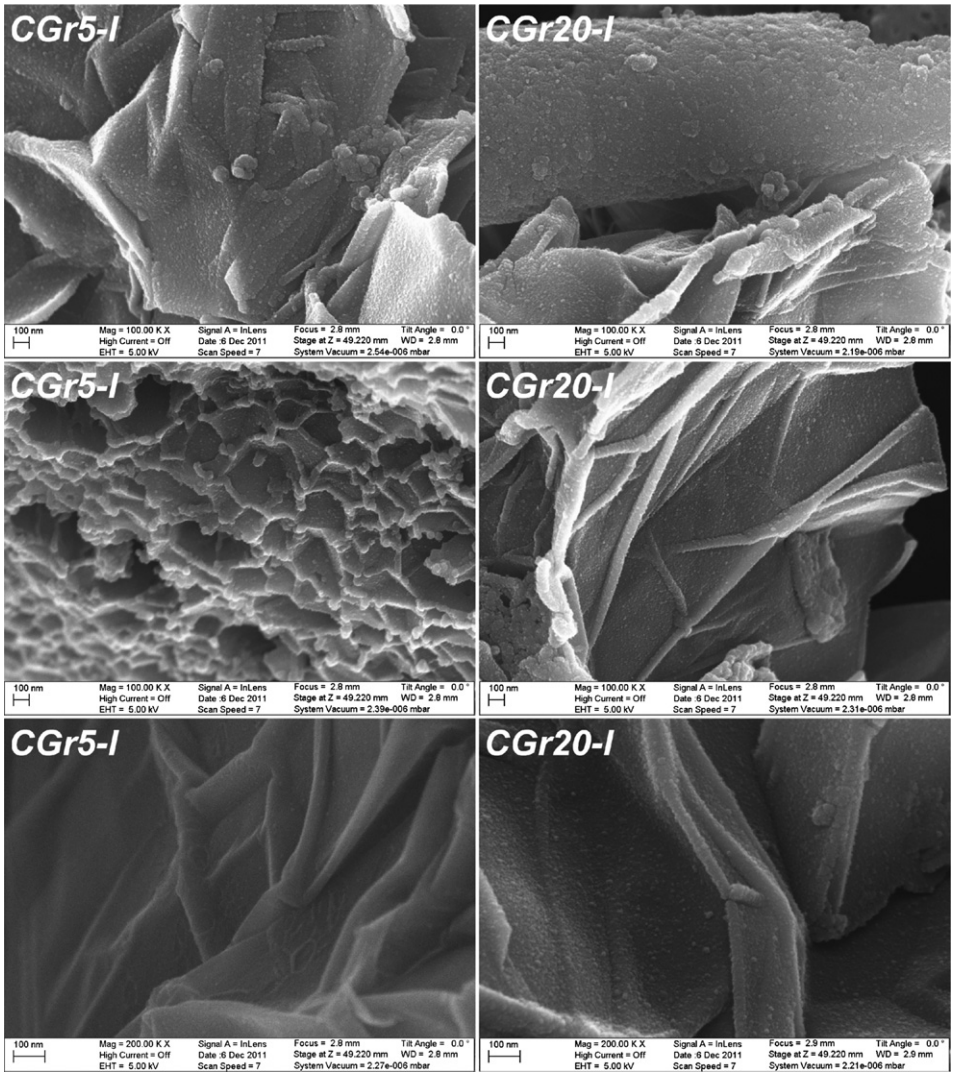

Fig. 5. SEM images of the composites.

reactions at close potential values should lead to the rectangular smooth CV curves. Interestingly, the humps are also revealed when the experiments are run in neutral electrolyte [10] and here also an addition of graphene decreases the effects.

The difference in the capacitance values between two electrolytes suggests either a marked effect of pseudocapacitance [20] and/or the presence of very small pores in our materials in which storage of hydrogen ions could be enhanced. When the CV curves in two electrode cells were measured again on the samples (CA – current applied) after the charging/discharging experiments, an increase in the performance was detected (Figs. 1 and 2). The comparison of the values calculated from CV curves to those of the initial samples is presented in Table 1. That quite significant increase (up to 17.7% in H_2SO_4 and more pronounced in the acid than in sodium sulfate) is attributed to the reduction of the composite surface in the irreversible reduction reaction on the electrode [44]. That reduction likely opens the pores of suitable sizes for the charge storage. Interestingly, this effect was not observed for the C-I or C-II. Apparently in the case of these carbons the reduced groups were located on the external surface or at the entrances to larger pores than those in the composites. The presence of the conductive graphene phase separating the nanoporous carbon units in the composite could help in electron transfer to the internal surface/small pores of the electrode where the surface groups can be reduced opening the entrances to the pores for charge storage.

The results discussed above suggest that the double layer capacitance (DLC) is the predominant mechanism of charge storage in our composites. It is generally accepted that the volume of small pores similar in size to the solvated ions is the most important for

Table 3
The ratios of the intensity of I_D/I_G of the Raman spectra band, contents of surface elements from EDX analysis, number of strongly acidic groups ($pK_a < 7$), weakly acidic ($pK_a > 7$) and total acidic groups.

Sample	I_D/I_G	C	O	S	Na	$pK_a < 7$	$pK_a > 7$	Total
		EDX (in atomic%)				(mmol g^{-1})		
Gr	0.50	92.2	7.8	–	–	0.097	0.172	0.269
C-I	1.75	91.9	7.1	1.0	–	0.377	0.311	0.688
C-II	–	93.6	6.0	0.4	–	0.060	0.204	0.264
CGr5-I	0.74	89.2	8.5	1.7	0.6	0.273	0.441	0.714
CGr5-II	–	92.1	5.7	2.2	–	0.140	0.397	0.537
CGr20-I	0.52	88.4	10.7	0.9	–	0.127	0.294	0.421
CGr20-II	–	90.8	9.1	0.2	–	0.117	0.246	0.363

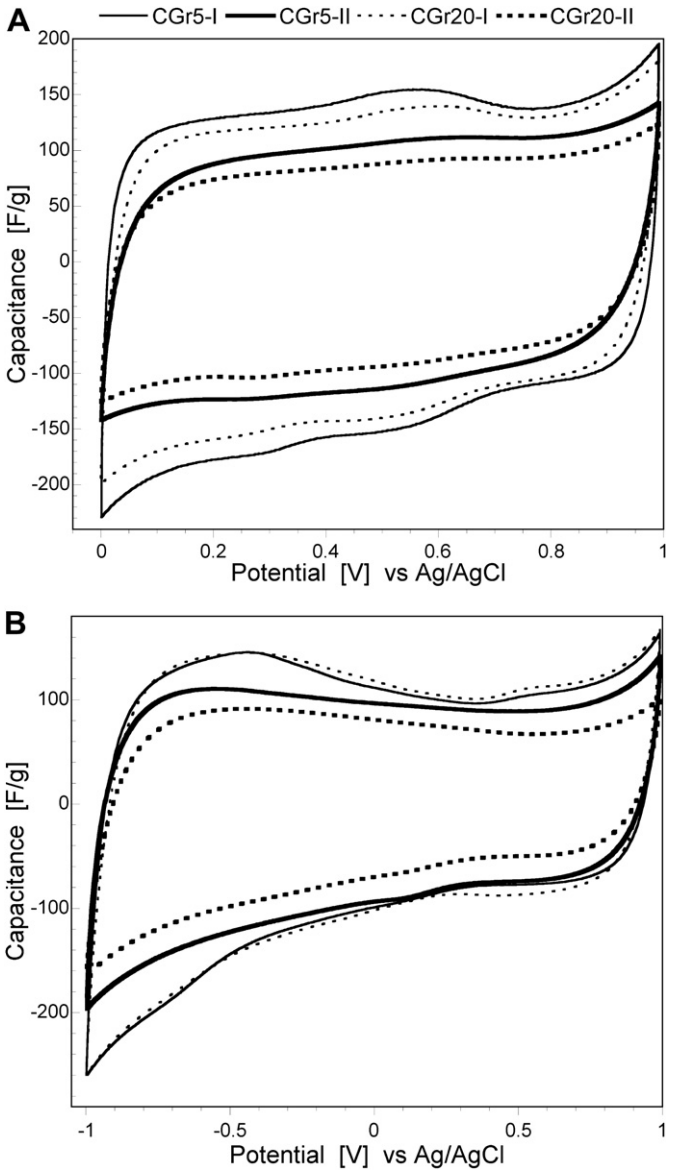

Fig. 6. Examples of the CV curves in three electrode cell *vs* Ag/AgCl at scan rate 5 mV s^{-1} in H_2SO_4 (A) and Na_2SO_4 (B) as electrolyte.

the DLC [38]. In Fig. 7 we plot the dependence of the gravimetric capacitance on the volume of pores smaller than: 0.7 nm, 1 nm, 2 nm. As seen, the smaller are the pores the better is the correlation coefficient. Moreover, the correlation is much better in Na_2SO_4 than in sulfuric acid. This is related to the stronger pseudocapacitive effects in the latter electrolyte [20]. The pseudocapacitance should also contribute more to the total capacitance in larger pores where the groups can exist.

Even though the volume in those small pores, <0.7 nm, differs up to 40% between the samples (Table 2), the capacitive performances measured are similar and the largest deviation of the C_g from the mean is 11% and the smallest is 1%. Therefore there must be other factors, which influence the performance. Assuming that the utilization of the pore space suitable for the double layer charge deposition is an important factor affecting the performance, and taking into account that the small pores should be the most active one, the ratio of the capacitance to the volume in pores smaller than 0.7 nm was calculated. We refer to this quantity as active pore space utilization. The highest values were obtained for the composites, especially in sulfuric acid and for the sample with 20% graphene. They are about 50% larger than those for the parent carbons. Taking into account the hypothesized above positive influence of graphene phase on the charge transfer to the small pores [19] the dependence of the active pore space utilization on the percent of graphene in our materials was analyzed. Even though the correlation coefficients for the plots presented in Fig. 8 are not perfect, for the samples obtained at 800 °C they are 0.99 in sulfuric acid and 0.99 in sodium sulfate. Interestingly after heating the correlation coefficients decrease to 0.71 and 0.87, respectively and thus the dependence weakens. An important factor contributing to the better linear trend for the samples heated at 800 °C than those obtained at 950 °C can be the presence of more functional groups which affect the wettability and thus ion transfer.

To further support the importance of conductivity for the capacitive behavior of our materials, the dependence of the active pore space utilization on the samples conductivity was plotted in Fig. 9. Even though the data scatter, some degree of correlation exists and it is better in sodium sulfate when the pseudocapacitance is less important. This is in agreement with the results of Hahn and coworkers [19] who suggested that DLC of carbon electrodes is governed by the electronic properties of the solids. If each series of materials obtained at 800 or 950 °C is considered the correlation coefficients improve. This is once again is an indication that there is another factor related to functional groups and wettability, which affects the DLC. Apparently heating at 950 °C and destroying some surface functional groups does not have the marked effects on

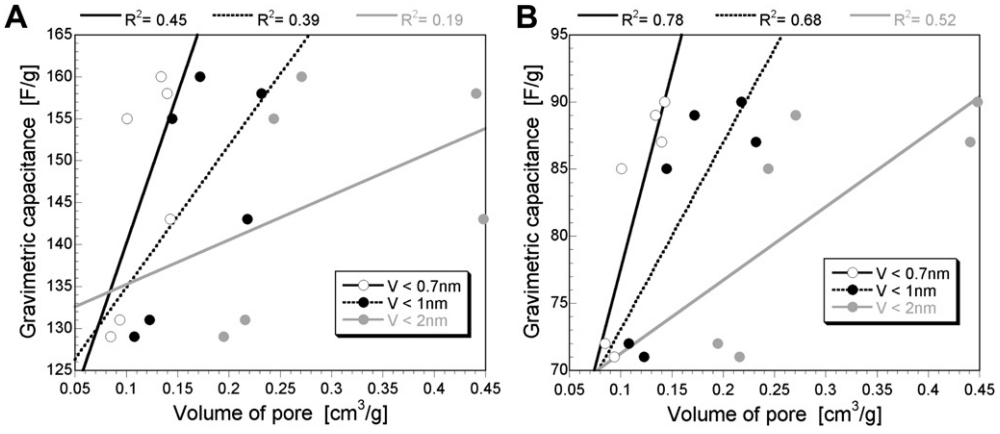

Fig. 7. Dependence of the capacitance in H_2SO_4 (A) and Na_2SO_4 (B) on the volume of the pores of different sizes.

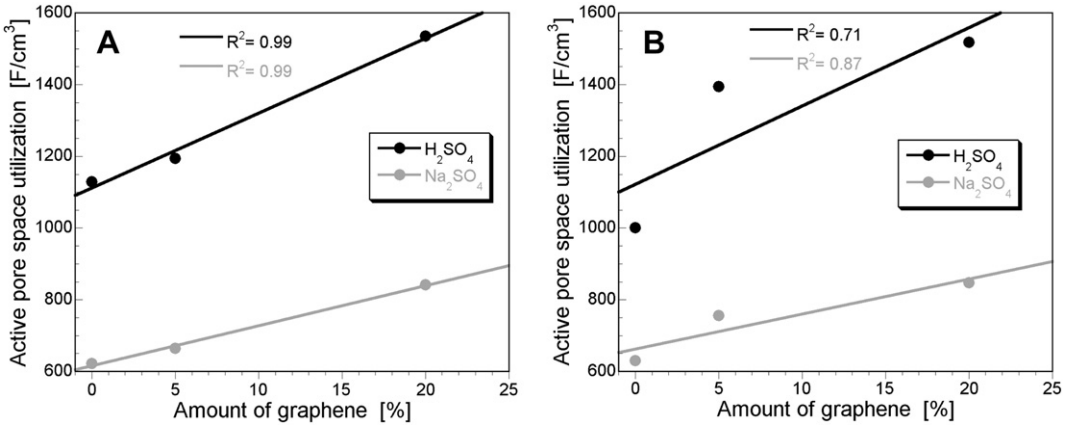

Fig. 8. Dependence of the active pore space utilization in H_2SO_4 and Na_2SO_4 on the amount of graphene for the initial (A) and heated at 950 °C (B) samples.

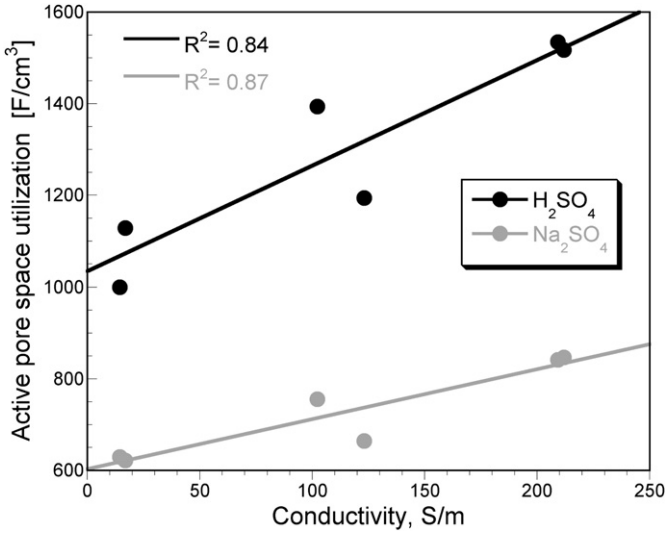

Fig. 9. Dependence of the active pore space utilization in H_2SO_4 and Na_2SO_4 on the samples' conductivity.

conductivity. It seems to be governed by the conductivity of the graphene phase (Table 2). Graphene addition to the carbon results in an order of magnitude improvement in the conductive properties.

4. Conclusions

The results presented in this paper showed the importance of the specific porosity and conductivity on the performance of nanoporous carbon-based materials as supercapacitors. That active pore space utilization was defined as gravimetric capacitance per unit pore volume in pores smaller than 0.7 nm. It was demonstrated that when double layer capacitance is a predominant mechanism of the charge storage, the degree of the active pore space utilization for that storage can be enhanced by increasing the conductivity of the carbons. It helps in efficient charge transfer to the small pores. In addition polar functional groups of carbons, even though some of them cannot contribute to pseudocapacitance, play a positive role for charge storage by increasing wettability of the surface.

Acknowledgment

This study was partially supported by CUNY Energy Institute SEED grant.

Appendix A. Supplementary information

Supplementary information related to this article can be found online at http://dx.doi.org/10.1016/j.jpowsour.2012.07.074.

References

[1] G. Salitra, A. Soffer, L. Eliad, Y. Cohen, D. Aurbach, J. Electrochem. Soc. 147 (2000) 2486–2493.
[2] L. Eliad, G. Salitra, A. Soffer, D. Aurbach, J. Phys. Chem. B 105 (2001) 6880–6887.
[3] J. Chmiola, G. Yushin, Y. Gogotsi, C. Portet, P. Simon, P.L. Taberna, Science 313 (2006) 1760–1763.
[4] C. Largeot, C. Portet, J. Chmiola, P.L. Taberna, Y. Gogotsi, P. Simon, J. Am. Chem. Soc. 130 (2008) 2730–2731.
[5] E. Raymundo-Piñero, K. Kierzek, J. Machnikowski, F. Béguin, Carbon 44 (2006) 2498–2507.
[6] C.O. Ania, V. Khomenko, E. Raymundo-Piñero, J.B. Parra, F. Béguin, Adv. Funct. Mater. 17 (2007) 1828–1836.
[7] A.G. Pandolfo, A.F. Hollenkamp, J. Power Sources 157 (2006) 11–27.
[8] D. Hulicova-Jurcakova, M. Seredych, G.Q. Lu, T.J. Bandosz, Adv. Funct. Mater. 19 (2009) 438–447.
[9] M. Seredych, D. Hulicova-Jurcakova, G.Q. Lu, T.J. Bandosz, Carbon 46 (2008) 1475–1488.
[10] M.P. Bichat, E. Raymundo-Pinero, F. Beguin, Carbon 48 (2010) 4351–4361.
[11] B.E. Conway, Electrochemical Supercapacitors: Scientific Fundamentals and Technological Applications, Kluwer Academic/Plenum, New York, 1999.
[12] M. Kawaguchi, A. Itoh, S. Yagi, H. Oda, J. Power Sources 172 (2007) 481–486.
[13] D. Hulicova, M. Kodama, H. Hatori, Chem. Mater. 18 (2006) 2318–2326.
[14] E. Frackowiak, G. Lota, J. Machnikowski, C. Vix-Guterl, F. Béguin, Electrochim. Acta 51 (2006) 2209–2214.
[15] D.-W. Wang, F. Li, L.-C. Yin, X. Lu, Z.-G. Chen, I.R. Gentle, G.Q.M. Lu, H.-M. Cheng, Chem. Eur. J. 18 (2012) 5345–5351.
[16] H.A. Andreas, B.E. Conway, Electrochim. Acta 51 (2006) 6510–6520.
[17] D. Hulicova-Jurcakova, M. Seredych, G.Q. Lu, T.J. Bandosz, Carbon 48 (2010) 1767–1778.
[18] H. Gomez, M.K. Ram, F. Alvi, P. Villalba, E. Stafanakos, A. Kumar, J. Power Sources 196 (2011) 4102–4108.
[19] M. Hahn, M. Baertschi, O. Barbieri, J.-C. Sauter, R. KoÆtz, R. Gallay, Electrochem. Solid-State Lett. 7 (2004) A33–A36.
[20] Y.-R. Nian, H. Teng, J. Electrochem. Soc. 149 (2002) A1008.
[21] C.W. Huang, C.H. Hsu, P.L. Kuo, C.T. Hsieh, H. Teng, Carbon 49 (2011) 895–903.
[22] B.-H. Kim, K.S. Yang, Y.A. Kim, Y.J. Kim, B. An, K. Oshida, J. Power Sources 196 (2011) 10496–10501.
[23] E. Raymundo-Piñero, M. Cadek, M. Wachtler, F. Béguin, ChemSusChem 4 (2011) 943–949.
[24] C.W. Huang, C.M. Chuang, J.M. Ting, H. Teng, J. Power Sources 183 (2008) 406–410.
[25] Y. Zhu, S. Murali, M.D. Stoller, K.J. Ganesh, W. Cai, P.J. Ferreira, A. Pirkle, R.M. Wallace, K.A. Cychosz, M. Thommes, D. Su, E.A. Stach, R.S. Ruoff, Science 332 (2011) 1537–1541.
[26] Z. Tai, X. Yan, J. Lang, Q. Xue, J. Power Sources 199 (2012) 373–378.
[27] J.D. Carruthers, J. Chung, I. Do, S. Letaj, M.A. Petruska, E.A. Sturm, D.A. Totir, Presented at CESEP'11, September 25–29, 2011, Vichy, France.
[28] L. Buglione, M. Pumera, Electrochem. Commun. 17 (2012) 45–47.
[29] L. Buglione, E.L.K. Chng, A. Ambrosi, Z. Sofer, M. Pumera, Electrochem. Commun. 14 (2012) 5–8.
[30] A. Ambrosi, A. Bonanni, Z. Sofer, J.S. Cross, M. Pumera, Chem. Eur. J. 17 (2011) 10763–10770.
[31] M. Seredych, R. Chen, T.J. Bandosz, Carbon 50 (2012) 4144–4154.

[32] D. Hines, A. Bagreev, T.J. Bandosz, Langmuir 20 (2004) 3388–3397.
[33] J. Jagiello, Langmuir 10 (1994) 2778–2785.
[34] J. Jagiello, T.J. Bandosz, J.A. Schwarz, Carbon 32 (1994) 1026–1028.
[35] J. Jagiello, J.P. Olivier, J. Phys. Chem. C 113 (2009) 19382–19385.
[36] M. Seredych, M. Khine, T.J. Bandosz, ChemSusChem 4 (2011) 139–147.
[37] J.L. Figueiredo, M.F.R. Pereira, M.M.A. Freitas, J.J.M. Órfão, Carbon 37 (1999) 1379–1389.
[38] C.-C. Hu, C.-C. Wang, F.-C. Wu, R.-L. Tseng, Electrochim. Acta 52 (2007) 2498–2505.
[39] F. Tuinstra, J.L. Koenig, J. Chem. Phys. 53 (1970) 1126–1130.
[40] R.C. Weast, J.A. Melvin, in: R.C. Weast, J.A. Melvin (Eds.), Handbook of Chemistry and Physics, CRC Press, Boca Raton, 1981, p. B-145.
[41] C. Petit, K. Kante, T.J. Bandosz, Carbon 48 (2010) 654–667.
[42] G. Kortum, W. Vogel, K. Andrusso, Dissociation Constants of Organic Acids in Aqueous Solutions, Butterworth, London, 1961.
[43] A.M. Puziy, O.I. Poddubnay, A. Martınez-Alonso, A. Castro-Muniz, F. Suarez-Garcıa, J.M.D. Tascon, Carbon 45 (2007) 1941–1950.
[44] R. Berenguer, J.P. Marco-Lozar, C. Quijada, D. Cazorla-Amoros, E. Morallon, Carbon 47 (2009) 1018–1027.